HHS Public Access

Author manuscript

Magn Reson Med. Author manuscript; available in PMC 2020 June 01.

Published in final edited form as:

Magn Reson Med. 2019 June ; 81(6): 3675–3690. doi:10.1002/mrm.27684.

Aortic 4d Flow MRI in under two minutes using compressed sensing, respiratory controlled adaptive k-space reordering, and inline reconstruction

Liliana Ma[1,2], **Michael Markl**[1,2], **Kelvin Chow**[1,4], **Hyungkyu Huh**[1], **Christoph Forman**[5], **Alireza Vali**[1], **Andreas Greiser**[5], **James Carr**[1], **Susanne Schnell**[1], **Alex Barker**[1], and **Ning Jin**[3]

[1]Department of Radiology, Feinberg School of Medicine, Northwestern University, Chicago, IL, United States

[2]Department of Biomedical Engineering, Northwestern University, Chicago, IL

[3]Cardiovascular MR R&D, Siemens Medical Solutions USA, Inc., Cleveland, OH, United States

[4]Cardiovascular MR R&D, Siemens Medical Solutions USA, Inc., Chicago, IL, United States

[5]Siemens Healthcare, Erlangen, Germany

Abstract

Purpose: To evaluate the in-vitro and in-vivo accuracy and feasibility of a free-breathing 4D flow technique using compressed sensing (CS), where 4D flow imaging of the thoracic aorta is performed in under 2 minutes with inline image reconstruction on the MRI scanner in less than five minutes.

Methods: 10 in-vitro 4D flow MRI scans were performed (9 CS acceleration factors [R=5.4-14.1], one GRAPPA R=2). Based on in-vitro results, CS-accelerated 4D flow of the thoracic aorta was acquired in 20 healthy volunteers (38.3±15.2 years old) and 11 patients with aortic disease (61.3±15.1 years) with R=7.7. A conventional 4D flow scan was matched for spatial coverage and temporal resolution.

Results: CS depicted similar hemodynamics to conventional 4D flow in-vitro, and in-vivo, with >70% reduction in scan time (volunteers: 1:52±0:25 vs. 7:25±2:35 minutes). Net flow values were within 3.5% in healthy volunteers, and voxel-by-voxel comparison revealed good agreement (bias ±LOA=−0.007±0.154 m/s). CS significantly underestimated peak velocities and peak flow in both volunteers and patients (*volunteers*: PV, - 16.2% to −9.4%, peak flow: −11.6 to −2.9%, *patients*: PV, −11.2 to −4.0%; peak flow, −10.2 to −5.8%).

Conclusion: Aortic 4D flow with CS is feasible in under two minutes with less than 5 minutes of inline reconstruction time. CS produced significant underestimation of peak flows and velocities, however, these were within 10-15% of conventional 4D flow-derived values. This technique may thus help shift 4D flow imaging into clinical practice for comprehensive assessment of 3D hemodynamics.

Name and complete address of correspondence: Ning Jin, ning.jin@siemens-healthineers.com.

Intro:

3D CINE phase-contrast MRI (also known as “4D flow MRI”) enables quantification and visualization of blood flow dynamics over the cardiac cycle. Advantages of 4D flow MRI compared to standard techniques such as 2D phase contrast (PC) MRI or Doppler echocardiography include this visualization of complex cardiovascular 3D hemodynamics and retrospective flow quantification at any location in the data volume.[1-4] Several studies have shown that 4D flow MRI can provide new insights in the relationship between 3D hemodynamics and the development of aortic pathologies. For example, recent 4D Flow MRI studies have shown that bicuspid aortic valve-mediated changes in aortic hemodynamics were significantly associated with the aortic dilatation phenotype and aortic wall degeneration on tissue histopathology, suggesting a physiologic mechanism by which valve abnormalities can influence the development of aortic disease.[5-9] However, clinical applications are still limited by the characteristically long scan times associated with multi-dimensional imaging (3D spatial and velocity-encoding, time-resolved over the entire cardiac cycle). Parallel imaging techniques like GRAPPA and SENSE are commonly used in 4D flow imaging to provide 2- to 3-fold acceleration, however these techniques still result in scan times of 5-15 minutes. Recent and ongoing developments in advanced imaging techniques have further reduced scan times, by [1] incorporating radial sampling patterns (PC-VIPR[10]), [2] exploiting spatio-temporal correlations [k-t SENSE, k-t BLAST[11], and PEAK-GRAPPA[12]] to achieve acceleration rates of R ~ 5, and [3] using sparse sampling patterns (e.g. k-t PCA[13]) to push acceleration rates even further.

In the last decade, compressed sensing (CS), which exploits the inherent compressibility of MRI data, has been combined with parallel imaging to achieve even higher acceleration rates that may put 4D flow into the realm of clinical feasibility.[14-20] To date, a number of preliminary studies have reported the application of CS to 4D flow imaging using a variety of sampling patterns. Dvyorne et al. achieved acceleration factors of 6, using a spiral sampling pattern to achieve 4D flow coverage of the abdomen in a single breathhold,[21] Hsiao et al. successfully applied a variable-density Poisson cartesian sampling pattern to a pediatric population,[22] and more recently, Cheng et al. combined variable density cartesian sampling with radial view-ordering (VRad) and CS to achieve acceleration factors of ~10.6. However, while the results of these studies have shown significant improvements in scan time, they were limited by offline reconstruction times, usually on the order of 3+ hours, making implementation into most clinical workflows difficult.

Thus, we propose a prototype 4D flow technique using L1-regularized wavelet-based compressed sensing and Respiratory Controlled Adaptive k-space Reordering (ReCAR), where 4D flow imaging of the thoracic aorta is performed in under 2 minutes with inline image reconstruction on the MRI system platform in less than five minutes. Therefore, the purpose of this study was to systematically investigate the accuracy and feasibility of CS-accelerated 4D flow MRI in comparison to conventional 4D flow based on in-vitro flow phantom experiments and in-vivo studies in healthy volunteers and patients with aortic valve disease.

Methods:

CS accelerated 4D flow MRI

Pulse sequence: A CS accelerated 4D flow MRI sequence was implemented using retrospective electrocardiographic-gating and symmetric, four-point velocity encoding (figure 1A). 4D flow data were acquired during free breathing using navigator-gating and Respiratory Controlled Adaptive k-space Reordering (ReCAR), where the diaphragm position was used to acquire central k-space at end-expiration and peripheral k-space during inspiration (figure 1C).[23,24] This technique included a previously-described, variable-density, Cartesian spiral phyllotaxis sampling pattern, with sampling patterns rotated between successive cardiac time frames to form a fully-sampled center for coil-sensitivity estimation, for use in the reconstruction.[25] All scans were acquired on a 1.5 T system (Aera, Siemens Medical Systems, Erlangen, Germany).

Image Reconstruction: Inline CS reconstruction was implemented based on a previously described framework[26] by solving the following optimization problem:

$$\{\mathbf{x}_t\}_{t=1,\ldots,T} = \operatorname{argmin}_{\{\mathbf{x}_t\}} \sum_{t=1}^{T} (\|\mathbf{A}_t\mathbf{x}_t - \mathbf{y}_t\|_2^2 + \lambda_\sigma \|\mathbf{W}_\sigma \mathbf{x}_t\|_1) + \lambda_\tau \|\mathbf{W}_\tau \{\mathbf{x}_1^\intercal, \ldots, \mathbf{x}_T^\intercal\}^\intercal\|_1 \quad (1)$$

where $\mathbf{x_t}$ denotes the frames to be reconstructed for all time points, $\mathbf{A_t}$ is the system matrix for each time point, *t*, consisting of the Fourier transform, sampling pattern, and coil sensitivity profiles for the local receiver coil elements and $\mathbf{y_t}$ denotes the measured data for each time point. Spatio-temporal L1 regularization was performed using a Haar wavelet transform where $\mathbf{W}_\sigma$ and $\mathbf{W}_\tau$ are represent spatial and temporal Wavelet transforms, and $\boldsymbol{\lambda_\sigma}$ and $\boldsymbol{\lambda_\tau}$ are the spatial and temporal regularization parameters, respectively. Equation [1] was solved using a FISTA optimization, and the reconstruction was fully integrated on a standard clinical scanner reconstruction system (Tesla K10 GPU).[27] The reconstruction parameters included 30 FISTA iterations with, $\boldsymbol{\lambda_\sigma} = 0.0015$ and $\boldsymbol{\lambda_\tau} = 5\boldsymbol{\lambda_\sigma}$. The regularization parameter $\boldsymbol{\lambda_\sigma}$ was scaled to the maximum and minimum signals of the data. If a higher signal-to-noise ratio was determined, the percent regularization was correspondingly scaled down.

In-vitro flow phantom experiments

Pulsatile Flow Circuit and Flow Phantom: CS 4D flow MRI was systematically evaluated in an in-vitro flow phantom using an MRI-compatible pulsatile flow circuit, and a patient-based 3D-printed realistic aorta flow phantom with an 80% coarctation in the descending aorta as described previously.[28] Briefly, realistic pulsatile flow was generated using a pneumatically driven ventricular assist device (VAD) and pump control unit (MEDOS, Germany). Pneumatic pressure was supplied to the VAD using a pump control unit outside the MR room. The VAD was directly attached to the 3D printed patient-specific model to mimic pulsatile flow entering the thoracic aorta. The pulsatile VAD can generated flow rates of up to 3.5L/S at frequencies of 69 “beats” per minute. Water doped with gadolinium-based contrast material was used as fluid in all experiments. All in-vitro 4D flow

measurements were gated to the pulsatile flow by a trigger signal generated by the pump control unit.

In-Vitro Phantom Measurements: A total of 10 in-vitro 4D flow MRI scans were performed (one standard 4D flow MRI with R=2, nine CS accelerated 4D flow with 9 different acceleration factors, R = 5.4-14.1). CS accelerated and conventional 4D flow MRI data were acquired with the following identical sequence parameters: TE/TR=2.1/4.8ms, BW= 455 Hz/voxel, flip angle = 15°, spatial resolution=2.3 mm^3, Venc = 350 cm/s. temporal resolution: 39 ms, 22 cardiac time frames.

In-Vitro Data Analysis: 4D flow MRI data preprocessing included noise-filtering, correction for Maxwell terms, second-order eddy current correction, and correction for velocity aliasing when necessary.[29] A 3D phase contrast MR angiogram (PC-MRA) was calculated from the 4D flow data and used to create a 3D segmentation of the thoracic aorta phantom (Mimics, Materialise, Leuven, Belgium). For both CS and non-CS acquisitions, nine 2D analysis planes were placed orthogonally along the entire aorta for quantification of regional peak velocities and time-resolved flow (figure 2Aa). To visualize blood flow in the entire aorta, systolic velocity maximum intensity projections (MIPs) were calculated by projecting the maximum absolute velocity onto a sagittal-oblique plane through the thoracic aorta (figure 2A)[30]. The CS data were temporally interpolated to the corresponding conventional 4D flow scan and voxel-by-voxel comparison of the CS versus conventional 4D flow scans was performed absolute velocities $|v|$, where $|v| = \sqrt{(v_x^2 + v_y^2 + v_z^2)}$.

In-vivo CS 4D flow Study

Study Cohort: CS accelerated and conventional 4D flow MRI of the thoracic aorta was prospectively acquired in 20 healthy volunteers (age = 38.3 ± 15.2 years old, range: 20-70 years, 10M/10F) and 11 patients with aortic valve disease (age = 61.3±15.1 years, range: 27-79 years, 9M/2F) from January to September 2018. Two patients were imaged after aortic valve replacement, five patients had bicuspid aortic valve (BAV) disease, two patients had aortic stenosis, one patient had moderate to severe aortic insufficiency, and one patient had aortic root enlargement with trace to mild regurgitation. The study was approved by the Institutional Review Board (IRB) of Northwestern University. Written informed consent was obtained from all volunteers and patients. Six of 10 patients underwent standard-of-care cardiothoracic MRI including contrast agent administration (Gadavist, Bayer Healthcare) and conventional 4D flow MRI. Informed consent was obtained in these patients for the additional CS acquisition.

In-Vivo Data Acquisition: For all subjects, a retrospectively-gated CS accelerated 4D flow sequence was acquired with an acceleration rate (R) of 7.7 (identified as optimal R based on phantom experiments). For comparison, a conventional, retrospectively-gated 4D flow sequence with R=2 GRAPPA acceleration with matched spatial/temporal resolution was acquired immediately after the CS accelerated 4D flow scan, or before in the case of the six patients who received 4D flow as part of their standard-or-care imaging. Pulse sequence parameters are summarized in table 1.

In-Vivo Data Analysis: 4D flow MRI data preprocessing included noise-filtering, correction for Maxwell terms, first-order eddy current correction, and correction for velocity aliasing when necessary.[29] A 4D flow-derived 3D PC MR angiogram was used to generate a 3D segmentation of the thoracic aorta (Mimics, Materialise, Leuven, Belgium). For regional flow quantification, nine 2D analysis planes were placed orthogonally along the entire aorta at the following anatomic landmarks: "root" placed at the aortic root, AAo1 and AAo2 spaced evenly between the Root and Arch1 plane, which was placed just before the brachiocephalic trunk; Arch2 placed just past the left subclavian artery, with Arch3, and Dao1-3 spaced evenly down the distal arch and descending aorta (figure 3A, *top right*). To account for the slightly different temporal resolutions of CS accelerated and conventional 4D flow MRI, all flow curves were interpolated to a temporal resolution of 10 ms. Aortic velocity MIPs were calculated and used to visualize blood flow (figure 3IA, 3IIA, *top*), as well as to quantify peak systolic velocities in three selected regions of interest in all subjects: the ascending aorta (AAo, defined from the aortic root to before the brachiocephalic trunk [BCT]), aortic arch (arch), and descending aorta (DAo) (figure 3A, *top left*). Time-resolved 3D streamlines and pathlines (Ensight, CEI, USA) were also generated to visualize blood flow (figure 3, *bottom*). Voxel-by-voxel comparison of the CS R=7.7 and conventional 4D flow scans was performed for each subject in the same manner as the in-vitro phantom comparison.

Statistical analysis:

All numbers are reported as mean ± standard deviation. The flow-time curves in all nine 2D analysis planes were averaged over all 20 volunteers for comparison of flow quantification. A Lilliefors test was used to evaluate parameter normality, and a non-parametric Wilcoxon rank-sum (RS) or a two-tailed, paired t-test was used accordingly to evaluate for differences between continuous parameters. Voxel-by-voxel comparisons included Bland-Altman analysis to establish the mean difference and limits of agreement (LOA) between the 4D flow techniques and calculation of a coefficient of variation (CV). Correlation between the two methods was assessed using orthogonal regression, with further evaluation using the intraclass correlation coefficient (ICC). A p-value <0.05 was considered statistically significant.

Results:

In-vitro:

Phantom results are summarized in figure 2 and tables 2 and 3. Systolic velocity MIPs in sagittal orientation for three representative CS acceleration factors (R=5.4, R=7.7, and R=14.1,figure 2A) demonstrate good agreement with conventional (GRAPPA, R=2) in-vitro 4D flow MRI. Flow quantification at representative 2D analysis planes (figure 2B) depict similar flow curve shapes between techniques, with noticeable but mild underestimation of peak flow in the CS acquisition, which was most perceptible in the descending aorta (DAo3). As delineated in table 2, relative change in peak flow (% differences between CS accelerated and conventional 4D flow MRI) across all 9 acceleration factors was Root: 0.5 to 2.7%, AAo (2 planes): −12.6 to −4.3%, Arch (3 planes): −13.1 to −0.4%, Dao (3 planes): −1.9 to 1.2%. The average relative change in net flow in the entire aorta was −10.0 to 7.6%

(table 2). Peak velocity quantified over the nine 2D analysis planes also showed an underestimation compared to conventional 4D flow (Root: −9.3 to 3.7%, AAo : −22.5 to −5.1 %, Arch: −16.7 to −0.6%, Dao: −19.9 to 1.3%).

Figure 2C-D shows Bland-Altman voxel-by-voxel comparisons and correlation plots for absolute aortic velocities for one representative acceleration factor (R=7.7) vs. conventional 4D flow MRI (GRAPPA with R=2) Bland Altman (figure 2C) and correlation analysis (figure 2D) indicate good-excellent agreement between both techniques as summarized in Table 3 which includes findings for experiments with all 9 acceleration factors. Bland-Altman analysis revealed mean differences with a small negative bias (<0.01 m/s) and low limits of agreement (<0.09 m/s). In addition, ICCs indicate a strong correlation between the techniques with high ICC (0.990-0.993) and slope close to unity (0.98-1.00). An acceleration rate of R=7.7 was reliable in producing results with an underestimation in parameters of interest of <15%, and thus this acceleration rate was subsequently chosen for the healthy control and patient cohorts.

Healthy Controls:

For the 10 healthy control subjects, total scan time for in-vivo CS 4D flow with R=7.7. was significantly reduced compared to conventional 4D flow MRI (1.9±0.3 min vs. 7.7±3.6 min, p<0.005). Representative blood flow visualization (systolic streamlines, velocity MIP), flow curves (Figure 3.IB), and voxel-by-voxel Bland Altman (figure 3.IC) composition shown in figure 3 indicate similar hemodynamic patterns for CS and conventional in-vivo 4D flow MRI (figure 3.IA). These findings were confirmed by quantitative comparisons of aortic in-vivo flow and velocities as summarized in figure 4 and Table 4. Flow-time curves for all 9 analysis planes (figure 4) for show good agreement between CS and conventional 4D flow MRI. Similar to in-vitro flow phantom findings, significant differences (indicated by * in Figure 4) between techniques were concentrated at the peaks of the flow waveforms as well as at the transition to diastole. As depicted in figure 5, peak velocities were significantly underestimated by CS compared to conventional 4D flow (*Conventional*, AAo: 1.55±0.18 m/s, Arch: 1.21±0.23 m/s, DAo: 1.31±0.25 m/s; *CS*, AAo: 1.38±0.17 m/s, Arch: 1.07±0.19 m/s, DAo: 1.10±0.23 m/s, p<0.001). Time-resolved flow analysis revealed a significant decrease in peak flow at the Root and in the Arch and DAo in the CS acquisition (Root: −7.6%, AAo: −8.7 to −2.9%, Arch: −9.0 to −7.8%, DAo: −11.6 to −8.4%, p<0.01). Net flow values of the CS acquisition were within 3.5 % of those of the conventional 4D flow acquisition in all 9 2D analysis planes.

Voxel-by-voxel comparison between CS and conventional 4D flow velocities across all 20 subjects revealed good agreement with small mean differences (−0.007±0.007 m/s) and limits of agreement (LOA = 0.154±0.0256 m/s). In addition, correlation analysis demonstrated strong and significant relationships between CS accelerated and conventional 4D flow MRI, with slope with a −4% deviation from unity (slope = 0.96±0.036, intercept=0.003±0.005 cm/s, ICC =0.93±0.02, p<0.01 for all volunteers).

Patient cohort:

CS 4D flow with R=7.7 and conventional 4D flow data were successfully acquired in 10 patients with aortic valve disease in 1:50±0:25 minutes vs. 7:13±2:39 minutes ($p<0.001$), respectively. 3D blood flow visualization using diastolic streamlines and systolic velocity MIPs in a patient with a prosthetic aortic valve (figure 3.II) indicate that CS and conventional 4D flow captured similar hemodynamic patterns (figure 3.IIA), with systolic MIPs depicting high velocity outflow jets, and diastolic streamlines depicting complex recirculating helical flow throughout the entire aorta. Cumulative flow and velocity quantification across all 10 patients is summarized in table 4 and figure 5. Peak velocities were significantly underestimated by CS compared to conventional 4D flow, in the arch and DAo (*Conventional*, AAo: 3.06 ± 1.21 m/s, Arch: 1.35 ±0.33 m/s, DAo: 1.09 ± 0.23 m/s; *CS*, AAo: 2.86 ± 0.91 m/s, Arch: 1.19 ± 0.23 m/s, DAo: 1.00 ± 0.26 m/s, $p<0.05$). Peak velocities were significantly greater in patients than volunteers in the AAo when comparing both conventional 4D flow- and CS-derived values ($p<0.02$). Net flow values differed significantly between the methods in the Arch2 ($p=0.02$), with a 9.3 ± 10.73%, 15.6 ± 19.9%, and −9.3 ± 7.5% difference from conventional 4D flow, respectively. Peak flow was significantly decreased in Arch1, Arch2, and DAo1-3 ($p<0.03$).

Voxel-by-voxel analysis of aortic velocities across all 10 patients revealed good agreement between techniques, with a mean difference of −0.0020±0.01 m/s and 0.233±0.083 m/s LOA. Correlation analysis revealed a strong correlation between conventional and CS 4D flow with wider standard deviations compared to the volunteers (slope=0.958 ±0.035, intercept=0.011±0.011 m/s, ICC = 0.89±0.08, $p<0.01$).

Discussion:

While the utility of 4D flow MRI in evaluating cardiovascular pathologies has long been investigated and supported, its clinical implementation is typically hindered by long scan times and complicated reconstruction workflows. Here, we developed a highly accelerated 4D flow technique using L1-regularized wavelet-based compressed sensing and Respiratory Controlled Adaptive k-space Reordering (ReCAR). The feasibility and performance of this technique was assessed in-vitro, on an aortic coarctation pulsatile flow phantom, as well as in 20 healthy volunteers and 11 patients with varying aortic diseases. We have demonstrated that (1) CS 4D flow MRI enabled significant and substantial acceleration of an aortic 4D flow acquisition (<2 minutes vs. 7-12 min); (2) full image reconstruction on the scanner allowed for immediate analysis and interpretation (3) voxel-by-voxel velocity comparison between CS and standard CS 4D flow MRI demonstrated good-excellent agreement; and (4) CS 4D flow MRI demonstrated underestimation of peak flow and peak velocities within 5-15%.

In-vitro experiments demonstrated that the use of CS with both spatial and temporal undersampling predictably led to an underestimation of hemodynamic parameters when compared to 4D flow MRI (−13.1% to 2.7% deviation from GRAPPA peak flow, −22.5% to 1.3% difference in peak velocity over all acceleration factors). However, while this underestimation appeared to become more severe with higher acceleration factors, even the maximum evaluated acceleration of R =14.1 resulted in good-to-excellent qualitative and

quantitative depiction of hemodynamics compared to conventional 4D flow (similar systolic flow patterns, flow curves follow similar shapes), with agreement in conventional 4D flow in both time-resolved and time-averaged hemodynamic indices, which were generally within 15%. Consistent flow patterns and thus stability of the in-vitro experiment allowed for ideal conditions for a voxel-by-voxel comparison, which further supported agreement between the techniques. In-vivo studies demonstrated similar results, with volunteer peak velocities and peak flows generally within 12% of conventional 4D-flow derived values. In patients with aortic valve disease, flow parameter variability and relative difference (%) compared to conventional 4D flow were higher than in volunteers. This result could be explained by the heterogeneity of the patient cohort. While all patients had a history of aortic valve disease, their presentations ranged from post-aortic valve replacement, to severe aortic stenosis, to aortic insufficiency. In addition, 3D phase-contrast techniques are inherently limited by the need to set a velocity sensitivity (venc). In patients with aortic valve stenosis, a higher venc (up to 500 cm/s) was needed to capture high peak velocities at the root and AAo. As a result, increased velocity noise coupled with the CS reconstruction could potentially account for the larger deviations in net flow and peak velocities in these patients. Further, the small sample size should be considered when evaluating statistical relationships. One patient had significant velocity aliasing in the ascending aorta. While most of this could be corrected, there was residual aliasing that affected the area of the plane at the aortic root, and thus patients' data was left out of the averaged flow and statistical analyses for the plane at the aortic root. Nonetheless, it is important to note that the deranged aortic flow patterns associated with aortic valve disease was fully captured in all patients. For example, patients with aortic valve disease presented with significantly increased ascending aortic peak velocities for both CS and conventional 4D flow MRI.

Other studies have also explored the combination of advanced imaging acceleration techniques and 4D flow MRI, including radial sampling schemes (PC-VIPR[10]) and multidimensional k-t accelerated parallel imaging schemes (k-t BLAST[11], PEAK-GRAPPA[12], k-t PCA[13]). Table 5 provides a concise summary of findings from this study compared to recent publications investigating highly accelerated 4D flow MRI, including MR imaging parameters and most relevant finings. For example, radial imaging with 3D PC vastly undersampled isotropic projection reconstruction (PC-VIPR) allowed high acceleration factors while maintaining good image quality.[31] PC-VIPR studies demonstrated good agreement with 2D PC MRI both in-vitro and in-vivo (R^2 = 0.99 and R^2=0.97, respectively) but a 6% underestimation in flow in in-vitro experiments using a pump with a known flow rate. K-t PCA is another technique that has been applied to accelerate 4D flow. Values derived from this technique were found to be highly correlated with those of 2D PC MRI (R^2 = 0.93 for stroke volumes), with some underestimation in peak flow in the AAo, superior vena cava, main pulmonary artery, and the left and right pulmonary arteries (−5.1% ±7.5%) in volunteers.[32] More recently, Bollache et al. explored a 2-minute aortic protocol using no respiratory navigation, k-t PEAK GRAPPA acceleration (R=5) with variable sampling patterns, and found underestimation in peak flow and peak velocity (Peak velocity, in-vitro, −22 to −0.8% underestimation, in-vivo [volunteers], −18% to 6.4%; *current study:* in-vitro, −22.5 to −3.7%, in-vivo [volunteers], - 16.2% to −9.4%).[33] These studies both used a similar in-vitro set up, and underestimations could be explained by undersampling in the

temporal dimension, but peak flow values were generally larger in the current in-vivo study, potentially because of the younger age of the volunteers, and the placement of the quantification planes. Moreover, while both studies incorporated free-breathing 4D flow techniques, Bollache focused on incorporating optimized sampling patterns into a previously developed k-t accelerated parallel imaging technique to reduce the need for navigator-gating, while the current study focused on incorporating navigator-gating into a k-t accelerated technique using CS. A smaller volunteer sample size and respiratory-motion effects could explain the higher standard deviations seen in Bollache's in-vivo data. It should also be noted that many of the other 4D flow acceleration techniques summarized in table 5 have been compared to 2D PC-MRI as the reference for flow imaging, but a technique that in itself has shown potential underestimation in flow parameters.[34]

Other groups have also reported on the combination of CS with 4D flow MRI and found similar underestimations in hemodynamic parameters (table 5). One of the first CS in 4D flow studies by Hsiao et al. successfully applied CS 4D flow MRI using a variable density Poisson-disk sampling pattern to a pediatric population.[22] However, this study focused on using 4D flow to qualitatively characterize cardiac shunts and valvular insufficiency, and no direct comparison was made with conventional 4D flow methods. Dvorne et al. successfully applied CS 4D flow using spiral sampling patterns to acquire abdominal 4D flow data in 24 heartbeats or a single breath hold.[21] Spiral 4D flow reconstruction took ~3 hours per subject offline on a dedicated computer. This group quantified 18 major abdominal vessels and found a significant underestimation in peak flow and peak velocity in CS compared to cartesian 4D flow. The increased severity of the underestimation may be due to the small size of abdominal vessels, which are likely more difficult to segment and limited by fewer voxels per region of interest than the thoracic aorta used in our study. More recently, Cheng et al. successfully applied CS 4D flow using a radial view-ordering (VDRad) design, where cartesian ky-kz samples were ordered in variable-density spiral-like spokes, to pediatric patients with congenital heart anomalies with acceleration rates of 10.6 and offline reconstructions of ~1 hour.[35, 36] While these studies focused on comparing sampling patterns or flexibility in clinical applications due to flexible data binning and reconstruction schemes, the authors did note a lower average flow rate in their XD flow recon using 4 temporal bins (~0.25 L/min) compared to their an unbinned 4D flow (temporally averaged, ~0.35 L/min).

The main limitation of this study is the low number of subjects. Patient evaluations were limited to a heterogenous group of patients and a small overall sample size. Although the results are encouraging, further patient studies are warranted to identify the limitations of this technique and potential implementation improvements, as well as protocol changes that could alleviate differences from conventional 4D flow. For example, patients with complex hemodynamics may require different spatial or temporal regularization compared to the protocol that we developed based on healthy controls, or perhaps they may benefit greatly from an improved acquired spatial resolution. Moreover, an acceleration factor of 7.7 was chosen based on phantom experiments for all subsequent in-vivo studies. While we would have liked to test multiple acceleration factors in-vivo, it was difficult to fit these into allotted patient and volunteer scan times. Future work will explore more acceleration factors to find the limits of the protocol, a test-retest study, evaluation of image quality, evaluation in

different applications (i.e. intracardiac, abdominal, neurovascular), and further exploration of the protocol itself (acceleration factors, venc, resolution).

In conclusion, we have demonstrated that aortic 4D flow with ReCAR, variable density poisson-disk sampling, and CS is feasible in under two minutes with less than 5 minutes of reconstruction on the scanner. This technique may be essential in the shift of 4D flow imaging into clinical practice for comprehensive assessment of 3D aortic hemodynamics.

References

1. Dyverfeldt P, Bissell M, Barker AJ, Bolger AF, Carlhäll C-J, Ebbers T, Francios CJ, Frydrychowicz A, Geiger J and Giese D. 4D flow cardiovascular magnetic resonance consensus statement. Journal of Cardiovascular Magnetic Resonance. 2015;17:72. [PubMed: 26257141]
2. Stankovic Z, Allen BD, Garcia J, Jarvis KB and Markl M. 4D flow imaging with MRI. Cardiovascular diagnosis and therapy. 2014;4:173. [PubMed: 24834414]
3. Roldán-Alzate A, Francois CJ, Wieben O and Reeder SB. Emerging applications of abdominal 4D flow MRI. American Journal of Roentgenology. 2016;207:58–66. [PubMed: 27187681]
4. Markl M, Frydrychowicz A, Kozerke S, Hope M and Wieben O. 4D flow MRI. Journal of Magnetic Resonance Imaging. 2012;36:1015–1036. [PubMed: 23090914]
5. Bissell MM, Hess AT, Biasiolli L, Glaze SJ, Loudon M, Pitcher A, Davis A, Prendergast B, Markl M, Barker AJ, Neubauer S and Myerson SG. Aortic dilation in bicuspid aortic valve disease: flow pattern is a major contributor and differs with valve fusion type. Circ Cardiovasc Imaging. 2013;6:499–507. [PubMed: 23771987]
6. Frydrychowicz A, Markl M, Hirtler D, Harloff A, Schlensak C, Geiger J, Stiller B and Arnold R. Aortic hemodynamics in patients with and without repair of aortic coarctation: in vivo analysis by 4D flow-sensitive magnetic resonance imaging. Investigative radiology. 2011;46:317–325. [PubMed: 21285892]
7. Guzzardi DG, Barker AJ, Van Ooij P, Malaisrie SC, Puthumana JJ, Belke DD, Mewhort HE, Svystonyuk DA, Kang S and Verma S. Valve-related hemodynamics mediate human bicuspid aortopathy: insights from wall shear stress mapping. Journal of the American College of Cardiology. 2015;66:892–900. [PubMed: 26293758]
8. Hope MD, Hope TA, Crook SE, Ordovas KG, Urbania TH, Alley MT and Higgins CB. 4D flow CMR in assessment of valve-related ascending aortic disease. JACC: Cardiovascular Imaging. 2011;4:781–787. [PubMed: 21757170]
9. Mahadevia R, Barker AJ, Schnell S, Entezari P, Kansal P, Fedak PW, Malaisrie SC, McCarthy P, Collins J, Carr J and Markl M. Bicuspid aortic cusp fusion morphology alters aortic three-dimensional outflow patterns, wall shear stress, and expression of aortopathy. Circulation. 2014;129:673–82. [PubMed: 24345403]
10. Johnson KM, Lum DP, Turski PA, Block WF, Mistretta CA and Wieben O. Improved 3D phase contrast MRI with off-resonance corrected dual echo VIPR. Magnetic Resonance in Medicine: An Official Journal of the International Society for Magnetic Resonance in Medicine. 2008;60:1329–1336.
11. Baltes C, Kozerke S, Hansen MS, Pruessmann KP, Tsao J and Boesiger P. Accelerating cine phase-contrast flow measurements using k-t BLAST and k-t SENSE. Magnetic resonance in medicine. 2005;54:1430–1438. [PubMed: 16276492]
12. Jung B, Ullmann P, Honal M, Bauer S, Hennig J and Markl M. Parallel MRI with extended and averaged GRAPPA kernels (PEAK-GRAPPA): optimized spatiotemporal dynamic imaging. Journal of Magnetic Resonance Imaging. 2008;28:1226–1232. [PubMed: 18972331]
13. Giese D, Schaeffter T and Kozerke S. Highly undersampled phase-contrast flow measurements using compartment-based k–t principal component analysis. Magnetic resonance in medicine. 2013;69:434–443. [PubMed: 22528878]

14. Feng L, Axel L, Chandarana H, Block KT, Sodickson DK and Otazo R. XD-GRASP: Golden-angle radial MRI with reconstruction of extra motion-state dimensions using compressed sensing. Magnetic resonance in medicine. 2016;75:775–788. [PubMed: 25809847]
15. Feng L, Grimm R, Block KT, Chandarana H, Kim S, Xu J, Axel L, Sodickson DK and Otazo R. Golden-angle radial sparse parallel MRI: Combination of compressed sensing, parallel imaging, and golden-angle radial sampling for fast and flexible dynamic volumetric MRI. Magnetic resonance in medicine. 2014;72:707–717. [PubMed: 24142845]
16. Feng L, Srichai MB, Lim RP, Harrison A, King W, Adluru G, Dibella EV, Sodickson DK, Otazo R and Kim D. Highly accelerated real-time cardiac cine MRI using k–t SPARSE-SENSE. Magnetic resonance in medicine. 2013;70:64–74. [PubMed: 22887290]
17. Kim D, Dyvorne HA, Otazo R, Feng L, Sodickson DK and Lee VS. Accelerated phase-contrast cine MRI using k-t SPARSE-SENSE. Magnetic resonance in medicine. 2012;67:1054–1064. [PubMed: 22083998]
18. Lustig M, Donoho D and Pauly JM. Sparse MRI: The application of compressed sensing for rapid MR imaging. Magnetic resonance in medicine. 2007;58:1182–1195. [PubMed: 17969013]
19. Feng L, Coppo S, Piccini D, Yerly J, Lim RP, Masci PG, Stuber M, Sodickson DK and Otazo R. 5D whole-heart sparse MRI. Magnetic resonance in medicine. 2018;79:826–838. [PubMed: 28497486]
20. Tariq U, Hsiao A, Alley M, Zhang T, Lustig M and Vasanawala SS. Venous and arterial flow quantification are equally accurate and precise with parallel imaging compressed sensing 4D phase contrast MRI. Journal of Magnetic Resonance Imaging. 2013;37:1419–1426. [PubMed: 23172846]
21. Dyvorne H, Knight-Greenfield A, Jajamovich G, Besa C, Cui Y, Stalder A, Markl M and Taouli B. Abdominal 4D flow MR imaging in a breath hold: combination of spiral sampling and dynamic compressed sensing for highly accelerated acquisition. Radiology. 2014;275:245–254. [PubMed: 25325326]
22. Hsiao A, Lustig M, Alley MT, Murphy MJ and Vasanawala SS. Evaluation of valvular insufficiency and shunts with parallel-imaging compressed-sensing 4D phase-contrast MR imaging with stereoscopic 3D velocity-fusion volume-rendered visualization. Radiology. 2012;265:87–95. [PubMed: 22923717]
23. Bailes D, Gilderdale D, Bydder G, Collins A and Firmin D. Respiratory ordered phase encoding (ROPE): a method for reducing respiratory motion artefacts in MR imaging. J Comput Assist Tomogr. 1985;9:835–838. [PubMed: 4019854]
24. Markl M, Harloff A, Bley TA, Zaitsev M, Jung B, Weigang E, Langer M, Hennig J and Frydrychowicz A. Time-resolved 3D MR velocity mapping at 3T: improved navigator-gated assessment of vascular anatomy and blood flow. Journal of magnetic resonance imaging. 2007;25:824–831. [PubMed: 17345635]
25. Forman C, Piccini D, Grimm R, Hutter J, Hornegger J and Zenge MO. High-resolution 3D whole-heart coronary MRA: a study on the combination of data acquisition in multiple breath-holds and 1D residual respiratory motion compensation. Magnetic Resonance Materials in Physics, Biology and Medicine. 2014;27:435–443.
26. Wetzl J, Forman C, Wintersperger BJ, D'errico L, Schmidt M, Mailhe B, Maier A and Stalder AF. High-resolution dynamic CE-MRA of the thorax enabled by iterative TWIST reconstruction. Magnetic resonance in medicine. 2017;77:833–840. [PubMed: 26888549]
27. Liu J, Rapin J, Chang T-c, Lefebvre A, Zenge M, Mueller E and Nadar MS. Dynamic cardiac MRI reconstruction with weighted redundant Haar wavelets. ISMRM. 2012;20:178.
28. Lorenz R, Benk C, Bock J, Stalder A, Korvink J, Hennig J and Markl M. Closed circuit MR compatible pulsatile pump system using a ventricular assist device and pressure control unit. Magnetic resonance in medicine. 2012;67:258–268. [PubMed: 21630351]
29. Bock J, Kreher B, Hennig J and Markl M. Optimized pre-processing of time-resolved 2D and 3D phase contrast MRI data. Proceedings of the 15th Annual meeting of ISMRM, Berlin, Germany 2007;604.
30. Rose MJ, Jarvis K, Chowdhary V, Barker AJ, Allen BD, Robinson JD, Markl M, Rigsby CK and Schnell S. Efficient method for volumetric assessment of peak blood flow velocity using 4D flow MRI. Journal of Magnetic Resonance Imaging. 2016;44:1673–1682. [PubMed: 27192153]

31. Gu T, Korosec FR, Block WF, Fain SB, Turk Q, Lum D, Zhou Y, Grist TM, Haughton V and Mistretta CA. PC VIPR: a high-speed 3D phase-contrast method for flow quantification and high-resolution angiography. American journal of neuroradiology. 2005;26:743–749. [PubMed: 15814915]
32. Giese D, Wong J, Greil GF, Buehrer M, Schaeffter T and Kozerke S. Towards highly accelerated Cartesian time-resolved 3D flow cardiovascular magnetic resonance in the clinical setting. Journal of Cardiovascular Magnetic Resonance. 2014;16:42. [PubMed: 24942253]
33. Bollache E, Barker AJ, Dolan RS, Carr JC, van Ooij P, Ahmadian R, Powell A, Collins JD, Geiger J and Markl M. k-t accelerated aortic 4D flow MRI in under two minutes: Feasibility and impact of resolution, k-space sampling patterns, and respiratory navigator gating on hemodynamic measurements. Magnetic resonance in medicine. 2018;79:195–207. [PubMed: 28266062]
34. Bollache E, van Ooij P, Powell A, Carr J, Markl M and Barker AJ. Comparison of 4D flow and 2D velocity-encoded phase contrast MRI sequences for the evaluation of aortic hemodynamics. The international journal of cardiovascular imaging. 2016;32:1529–1541. [PubMed: 27435230]
35. Cheng JY, Hanneman K, Zhang T, Alley MT, Lai P, Tamir JI, Uecker M, Pauly JM, Lustig M and Vasanawala SS. Comprehensive motion-compensated highly accelerated 4D flow MRI with ferumoxytol enhancement for pediatric congenital heart disease. Journal of Magnetic Resonance Imaging. 2016;43:1355–1368. [PubMed: 26646061]
36. Cheng JY, Zhang T, Alley MT, Uecker M, Lustig M, Pauly JM and Vasanawala SS. Comprehensive Multi-Dimensional MRI for the Simultaneous Assessment of Cardiopulmonary Anatomy and Physiology. Scientific reports. 2017;7:5330. [PubMed: 28706270]
37. Schnell S, Markl M, Entezari P, Mahadewia RJ, Semaan E, Stankovic Z, Collins J, Carr J and Jung B. k-t GRAPPA accelerated four-dimensional flow MRI in the aorta: effect on scan time, image quality, and quantification of flow and wall shear stress. Magnetic resonance in medicine. 2014;72:522–533. [PubMed: 24006309]
38. Zaman A, Motwani M, Oliver JJ, Crelier G, Dobson LE, Higgins DM, Plein S and Greenwood JP. 3.0 T, time-resolved, 3D flow-sensitive MR in the thoracic aorta: impact of k-t BLAST acceleration using 8-versus 32-channel coil arrays. Journal of Magnetic Resonance Imaging. 2015;42:495–504. [PubMed: 25447784]

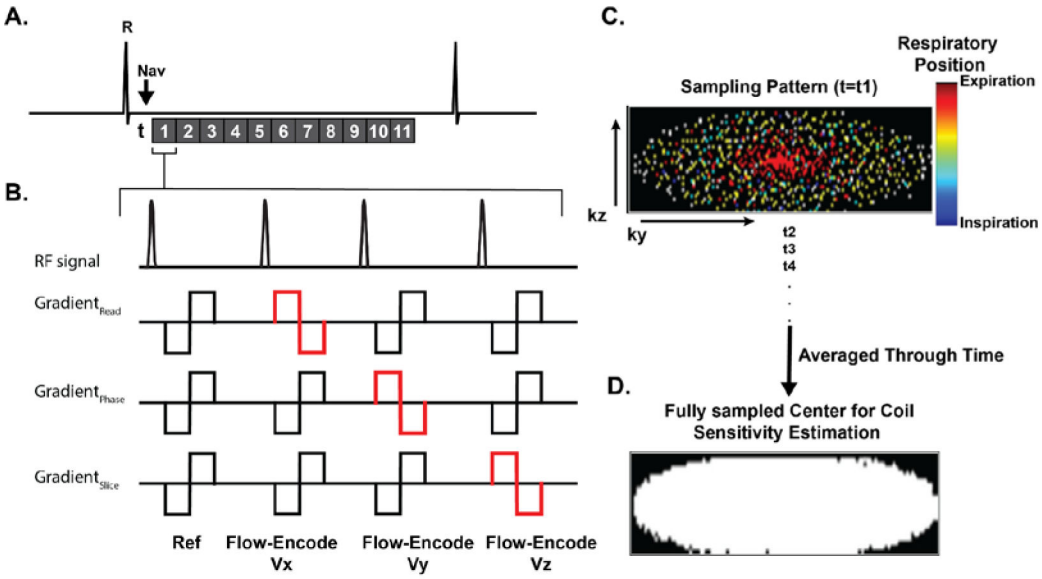

Figure 1:

CS Acquisition and Reconstruction. (A,B) Retrospectively gated flow acquisition using symmetric 4-point encoding gated to the cardiac cycle. Navigator echos (Nav) were played out after R-wave detection in the ECG tracing. Numbers (1-11) represent successive cardiac time frames(tn, n=1,2…11). Each time frame corresponds to a set of k-space data with x,y,z dimensions (kx-ky-kz). (C) shows ReCAR with a poisson disk sampling pattern in the kz/ky dimensions of a single time frame, that is subsequently rotated for each time frame (t_n). When all cardiac time frames are combined, they form a fully sampled center of k-space, (D) for coil sensitivity estimation.

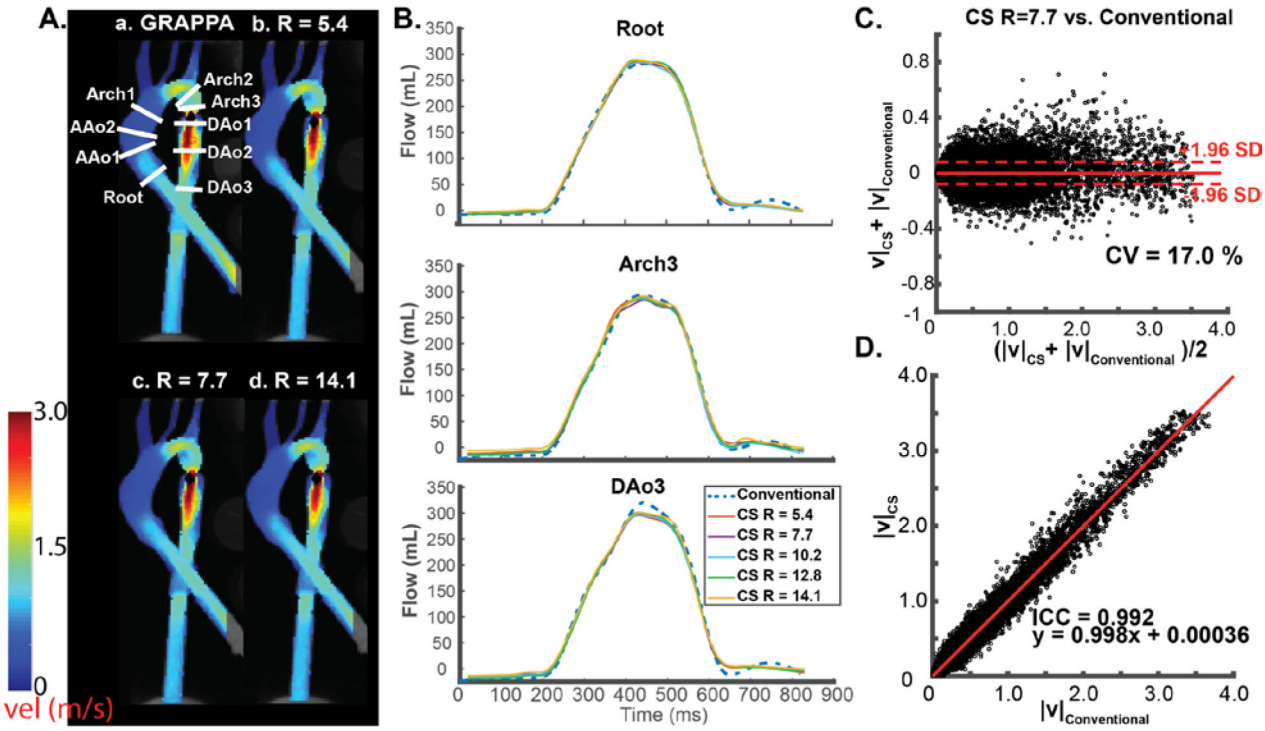

Figure 2:

In-vitro aorta flow phantom analysis. (A) Systolic velocity maximum intensity projections (MIPs) of conventional 4D flow (a) compared to CS accelerated 4D flow MRI with three representative acceleration factors (b-d). a, location of 9 2D analysis planes for quantification of peak velocities and flow-time curves. (B) Representative flow curves at three locations in the aorta for conventional 4D flow (dashed blue line, GRAPPA, R=2) compared to CS accelerated 4D flow with 5 different acceleration factors ranging from R=5.4-14.1. (C) Voxel-by-voxel Bland Altman comparison of absolute velocities in the entire aorta phantom between CS accelerated 4D flow with R=7.7 vs. conventional 4D flow. (D) Voxel-by-voxel orthogonal regression analysis between CS accelerated 4D flow with R=7.7 vs. conventional 4D flow.

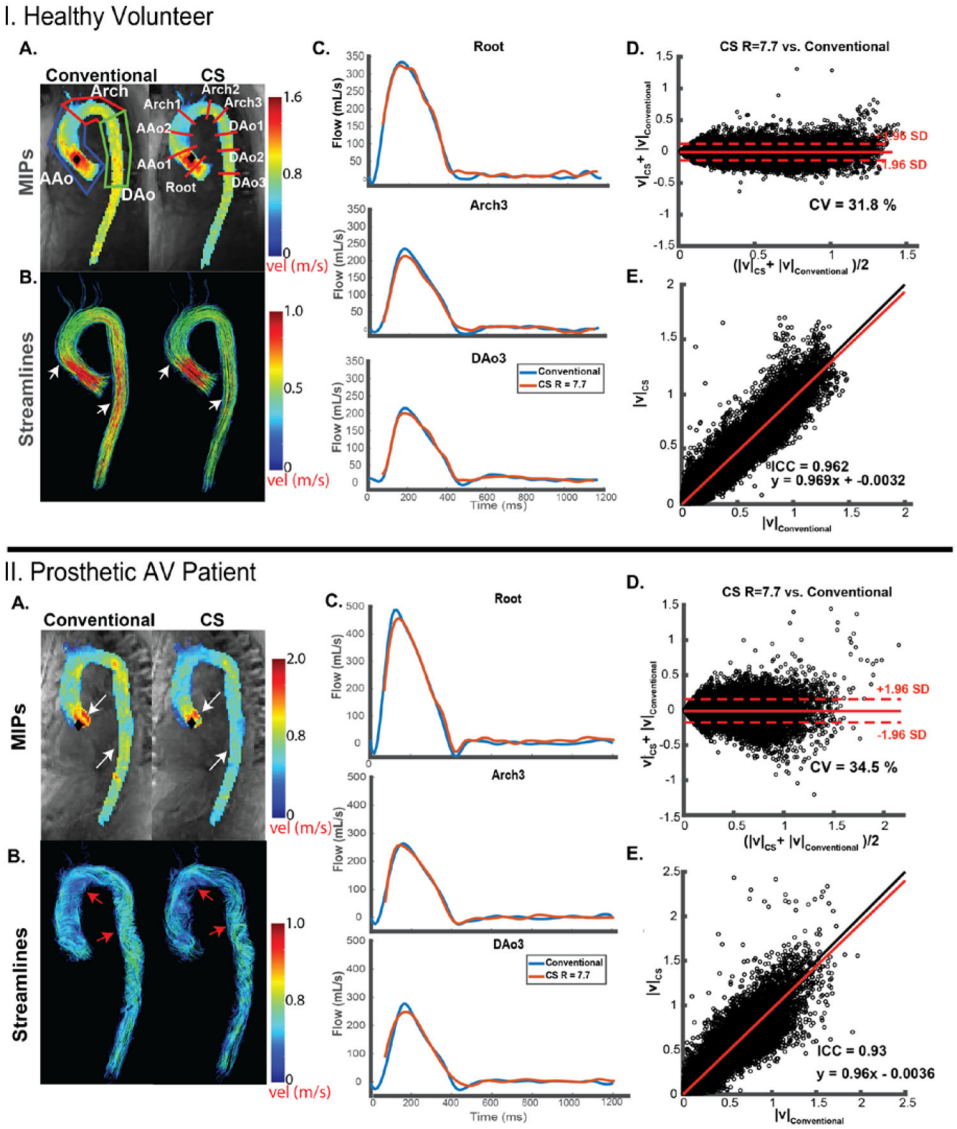

Figure 3:

Representative in-vivo aortic hemodynamics for a healthy volunteer (I) and patient (II). (A) Peak velocity maximum intensity projections (MIPs, top) and systolic (I) or diastolic (II) 3D streamlines (bottom) of conventional 4D flow (GRAPPA, R=2) and CS 4D flow (R=7.7). Black diamonds represent points of maximum velocity. Regions of interest (ROIs, top left) were used to quantify peak velocity in the ascending aorta (AAo), arch, and descending aorta (DAo). Nine 2D analysis planes at defined anatomic locations were used for flow quantification. Arrows indicate regions with visible differences between the two techniques. Note the underestimation in areas of high velocities in the ascending and descending aorta (white arrows). Prosthetic aortic valve (AV) patient diastolic streamlines depict complex helical flow in both techniques, with less dense streamlines in the CS accelerated 4D flow (red arrows). (B) Representative flow curves at three locations in the aorta for conventional 4D flow (blue line) compared to CS accelerated 4D flow (red line). (C) Voxel-by-voxel Bland Altman comparison of absolute velocities in the entire aorta between CS accelerated

4D flow vs. conventional 4D flow. (D) Voxel-by-voxel orthogonal regression analysis between CS accelerated 4D flow with R=7.7 vs. conventional 4D flow.

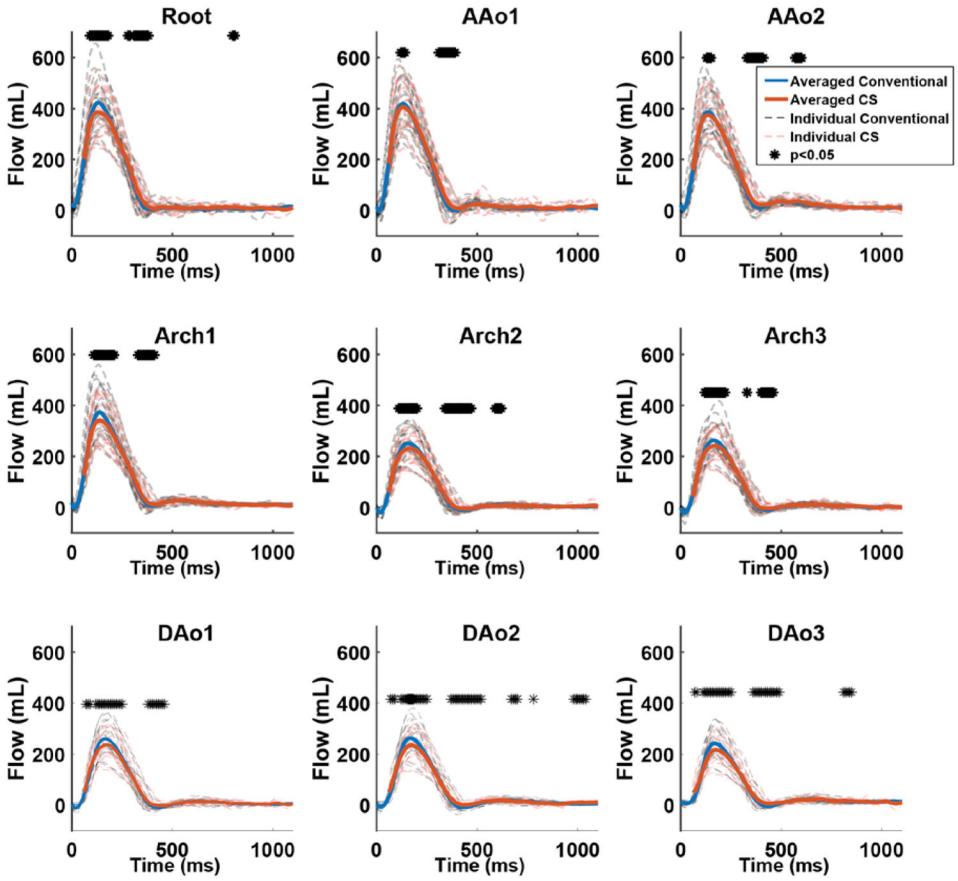

Figure 4:

Flow-time curves of all 20 healthy volunteers for all 9 2D analysis planes. Solid orange and blue lines represent flow curves averaged over all n=20 subjects for CS and conventional 4D flow, respectively. Dotted black and red lines represent flow curves for each individual volunteer (n=20). (*) above the curves represent time points with significant differences ($p<0.05$) between the conventional and CS accultured 4D flow acquisitions. Good agreement between conventional and CS 4D flow derived flow-time curves as well as mild peak flow underestimation by CS accelerated 4D flow can clearly be appreciated. Most pronounced differences were found at areas of peak flow or transitions to diastole.

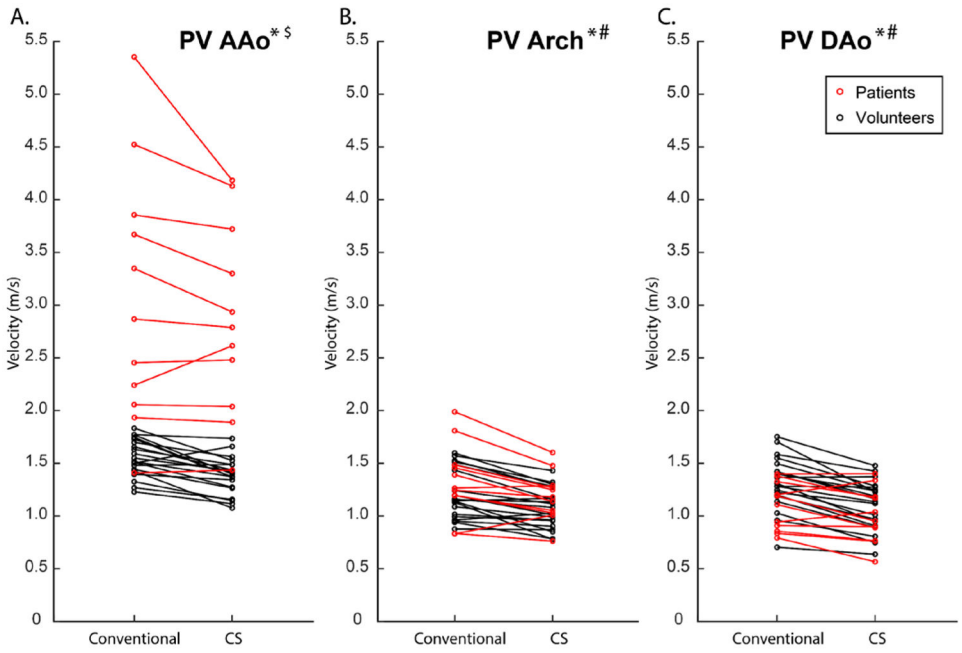

Figure 5:

Peak Velocities for conventional and CS 4D flow over all patients and volunteers in the ascending aorta (AAo), arch, and descending aorta (DAo). Graphs demonstrate a tendency to underestimate velocities in the CS 4D flow in all three regions of interest. Most patients (red circles) had some form of aortic stenosis due to their various aortic valve pathologies, and thus their peak velocities were higher than those of the volunteers in the AAo.

*significant differences between CS and conventional in volunteers

significant differences between CS and conventional in patients

$ significant differences between volunteers and patients

Table 1:

4D flow Imaging Parameters for all volunteers and patients. Notable differences in patient parameters are represented in parentheses.

	Conventional	**CS**
R	2	7.7
Scan Time (s)	460 ± 218 (433 ± 159)	116 ± 18 (110 ± 25)
Echo Time (ms)	2.3 (2.0-2.3)	2.3 (2.0-2.3)
Repetition Time	5.1 (4.8-5.1)	5.1 (4.8-5.1)
Temporal Resolution (ms)	40.0-45.3	38.1-44.5
BW	455	455
Flip angle (°)	7 (15 with contrast)	7 (15 with contrast)
Interpolated voxel size (mm^3)	2.4-2.5 × 2.4-2.5 × 2.4-2.9	2.4-2.5 × 2.4-2.5 × 2.4-2.9
Acquired voxel size (mm^3)	2.4-2.5 × 3.5-3.8 × 3.6-4.3	2.4-2.5 × 3.5-3.8 × 3.3-3.8
acquired matrix size	160 × 82 × 20	160 × 82 × 20
FOV (mm^3)	380-400 × 285-315 × 72-84	380-400 × 285-315 × 72-84
Venc (cm/s)	150 (150-500)	150 (150-500)
Reconstructed Cardiac Time Frames	18-32	17-31
Navigator Acceptance Window (mm)	8	8

Table 2:

In-vitro study results. Peak Flow, Peak Velocity, and Net Flow (top, middle, bottom) are presented for nine different acceleration factors ranging from 5.4 to 14.1 (left column), for 9 different 2D analysis planes from the root to the descending aorta (top row).

	Root	AAo1	AAo2	Arch1	Arch2	Arch3	DAo1	DAo2	DAo3
Peak Flow (mL/s)									
GRAPPA									
R = 2	282.9	303.8	304.4	292.0	286.0	292.6	294.2	349.0	320.6
R = 5.4	284.4	284.5	275.7	265.8	271.4	290.0	278.1	340.4	295.7
R = 6.4	285.3	288.2	277.2	264.7	273.7	290.0	293.6	328.6	301.8
R = 7.7	285.8	288.1	275.3	265.2	267.1	283.4	286.2	338.3	297.5
R =8.9	289.1	286.1	279.1	270.7	269.4	285.0	290.4	322.9	294.1
R = 10.2	285.0	284.0	290.0	265.0	265.8	287.4	293.0	342.4	295.4
R = 11.5	284.5	284.4	278.5	269.5	265.7	283.3	282.9	333.6	292.2
R = 12.8	289.6	282.7	266.1	259.1	267.0	285.3	284.7	324.7	301.1
R = 13.4	290.6	283.5	269.3	257.9	269.3	284.7	280.5	315.8	296.8
R = 14.1	288.8	284.2	267.4	253.8	266.5	291.2	297.6	328.1	299.8
Peak Velocity (m/s)									
GRAPPA									
R = 2	1.08	0.78	0.49	0.48	1.53	1.56	3.16	2.25	1.46
R = 5.4	1.04	0.73	0.42	0.42	1.51	1.42	3.15	2.11	1.27
R = 6.4	1.02	0.74	0.38	0.42	1.52	1.45	3.16	1.99	1.24
R = 7.7	1.01	0.68	0.43	0.44	1.50	1.40	3.13	2.08	1.23
R =8.9	1.00	0.71	0.42	0.45	1.48	1.39	3.20	2.04	1.24
R = 10.2	1.00	0.72	0.43	0.42	1.48	1.43	3.16	2.25	1.18
R = 11.5	0.98	0.72	0.39	0.43	1.47	1.38	3.02	1.82	1.18
R = 12.8	1.02	0.74	0.44	0.41	1.45	1.32	3.00	2.03	1.17
R = 13.4	1.00	0.69	0.42	0.44	1.46	1.39	3.00	2.13	1.18
R = 14.1	0.99	0.67	0.38	0.40	1.46	1.46	3.01	1.94	1.17
Net Flow (mL/cycle)									
GRAPPA									
R = 2	75.8	80.9	84.9	83.7	74.0	71.6	67.5	87.2	74.4
R = 5.4	75.9	78.0	80.0	81.7	71.9	73.6	69.9	82.0	71.8
R = 6.4	75.4	78.0	79.9	80.8	71.7	75.1	70.1	78.5	69.9
R = 7.7	75.9	80.2	83.5	81.6	71.4	71.3	70.3	83.0	72.9
R =8.9	76.0	82.1	86.8	88.4	71.1	70.6	68.2	79.6	72.7
R = 10.2	75.4	80.6	85.9	85.1	70.7	71.3	68.2	82.6	73.1
R = 11.5	77.2	83.1	86.1	85.9	70.5	71.2	69.4	79.7	71.8
R = 12.8	77.8	80.2	81.6	82.1	71.2	72.1	66.5	81.8	72.6
R = 13.4	78.0	80.6	80.7	81.5	72.9	74.2	68.1	79.8	71.8
R = 14.1	77.9	80.4	78.7	78.6	72.8	76.4	72.6	80.5	75.4

Table 3:

Voxel-by-Voxel Phantom Comparison. Bland-Altman analysis is presented with the mean difference and limits of agreement (LOA). CV= coefficient of variation.

Voxel-by-Voxel Analysis						
	Bland-Altman Analysis			*Correlation Analysis*		
	Mean difference (m/s)	***LOA (m/s)***	***CV(%)***	***Slope***	***Intercept***	***ICC***
R = 5.4	−0.0012	0.079	17.3	1.00	<0.001	0.993*
R = 6.4	>−0.001 & <0.001	0.076	16.7	1.00	−0.0012	0.993*
R = 7.7	>−0.001 & <0.001	0.078	17.0	1.00	<0.001	0.993*
R =8.9	<0.001	0.082	18.5	0.99	0.0023	0.992*
R = 10.2	<0.001	0.085	18.3	0.99	0.0015	0.991*
R = 11.5	>−0.001 & <0.001	0.087	18.7	0.99	0.0028	0.991*
R = 12.8	−0.0029	0.087	18.4	0.98	0.0014	0.991*
R = 13.4	−0.0022	0.089	19.2	0.98	0.0026	0.990*
R = 14.1	−0.0032	0.090	18.8	0.99	<0.001	0.990*

(*)means P<0.001 for correlation anayses ICC.

Table 4:

Volunteer (n=20) and patient (n=11) Peak Flow and Net Flow over all planes with corresponding % change in CS values relative to conventional 4D flow.

Volunteers (n=20)									
Peak Flow (mL/s)									
	Root*	***AAo1****	***AAo2****	***Arch1****	***Arch2****	***Arch3****	***DAo1****	***DAo2****	***DAo3****
GRAPPA R = 2	428 ± 98	426 ± 96	393 ± 92	379 ± 94	257 ± 55	270 ± 65	265 ± 57	268 ± 63	249 ± 58
CS R=7.7	393 ± 82	412 ± 90	378 ± 85	345 ± 81	237 ± 53	245 ± 557	243 ± 53	237 ± 58	222 ± 50
% Change in CS	**−7.6 ± 5.6**	**−2.9 ±6.7**	**−3.5 ± 7.1**	**−8.7 ± 4.9**	**−7.8 ± 6.8**	**−9.0 ± 6.7**	**−8.4 ± 6.4**	**−11.6 ± 6.2**	**−10.6 ± 5.1**
Net Flow (mL/s)									
	Root	***AAo1***	***AAo2***	***Arch1****	***Arch2***	***Arch3***	***DAo1***	***DAo2****	***DAo3***
GRAPPA R = 2	82 ± 17	83 ± 17	84 ± 18	79 ± 18	51 ± 12	53 ± 13	53 ± 12	55 ± 13	53 ± 13
CS R=7.7	83 ± 16	86 ± 17	86 ± 16	77 ± 17	50 ± 11	52 ± 13	52 ± 12	53 ± 12	53 ± 12
% Change in CS	**1.7 ± 7.6**	**3.3 ± 8.2**	**3.5 ± 7.6**	**−2.1 ± 5.0**	**−1.6 ± 10.1**	**−0.8 ± 7.3**	**−1.7 ± 6.9**	**−2.9 ± 5.4**	**−0.6 ± 5.9**
Patients (n=11)									
Peak Flow (mL/s)									
	Root	***AAo1***	***AAo2***	***Arch1****	***Arch2****	***Arch3***	***DAo1****	***DAo2****	***DAo3****
GRAPPA R = 2	444 ± 141	426 ± 109	426 ± 119	405 ± 102	248 ± 63	260 ± 67	269 ± 85	260 ± 74	253 ± 78
CS R=7.7	449 ± 145	436 ± 113	441 ± 107	370 ± 92	231 ± 63	257 ± 66	244 ± 75	236 ± 70	219 ± 71
% Change in CS	**1.1 ± 9.2**	**6.2 ± 10.4**	**7.2 ± 11.5**	**−6.3 ± 7.0**	**−5.9 ± 7.6**	**1.4 ± 10.7**	**−5.8 ± 5.5**	**−6.8 ± 6.9**	**−10.2 ± 9.4**
Net Flow (mL/s)									
	Root	***AAo1****	***AAo2****	***Arch1***	***Arch2****	***Arch3***	***DAo1***	***DAo2***	***DAo3***
GRAPPA R = 2	82 ± 17	80 ± 21	81 ± 22	79 ± 18	48 ± 11	46 ± 9	47 ± 10	49 ± 10	49 ± 10
CS R=7.7	77 ± 27	86 ± 27	90 ± 26	74 ± 19	44 ± 94	48 ± 9	45 ± 8	48 ± 11	49 ± 12
% Change in CS	**1.4 ± 12.5**	**7.1 ± 12.4**	**13.1 ± 20.5**	**−6.1 ± 9.8**	**−7.7 ± 8.9**	**3.6 ± 11.9**	**−3.7 ± 7.5**	**−1.0 ± 7.6**	**0.9 ± 8.1**

(*) indicates significant differences between CS accelerated and conventional 4D flow MRI ($p<0.05$). AAo = Ascending Aorta, Dao = Descending Aorta.

Table 5:

Previous evaluations in the literature of accelerated 4D flow. Second column lists “conventional” comparison method first, if applicable, and acceleration technique to be evaluated second. SR=spatial resolution, tempRes = temporalresolution

Study and Population	MRI Acquisitions	Main Relevant Findings
Current study n=20 healthy volunteers (mean age 38.3 [22-70] years) n=11 patients with aortic valve disease	1.5T: Aortic Acquisition **Navigator-gated cartesian 4D flow with retrospective gating and ReCAR:** SR=2.4-2.5 × 3.5-5.0 × 3.3-3.8mm^3 Temp Res: 40.0-45.3 ms Acquisition Time: 7.7 ± 3.6 min **k-t accelerated cartesian 4D flow with retrospective gating, ReCAr, and CS reconstruction:** SR=2.4-2.5 × 3.5-5.0 × 3.3-3.8Mm^3 Temp Res: 38.5-44.5 ms Acquisition Time: 1.9 ± 0.3 min	Peak Velocity: Volunteers: −16 to −10 % underestimation Patients: Peak Flow: Volunteers: −10.1 to −0.9% underestimation
Gu et al, AJNR 2005[31] n=6 (3 patients, 3 volunteers) all had contrast except one Flow phantom with controllable flow rate	1.5T Venc = 20 cm/s Intracranial acquisition **Cartesian 4D Flow:** acquired SR=0.95×0.95× 2.00 mm^3 TR/TE = 6.6 ms/18 ms Acquisition time= 7 min 22 sec unsure of R **PC VIPR** acquired SR = 0.63×0.63×0.63 mm^3 TR/TE = 7.57/17.34 ms Acquisition time varied from 3:50 to 7:30 min depending on FOV and number of radial projections	Flow validation resulted in R^2 = 0.99 in vitro and R^2=0.97 in vivo, but this was involving comparison to 2D PC. PC-VIPR had a 6% underestimation in phantom flow with known flow rates. Direct comparison to 4D flow MRI focused on qualitative evaluation
Hsiao Radiology 2012[22] n = 34 (mean 6, range 10 month to 21 years)	1.5T Venc = 120-350 cm/s whole heart **variable-density Poisson disk k-space undersampling:** acceleration 1.4×1.4 to 2.2×2.2 (ky-kz); SR = 1.02×1.34×2.30 mm^3 temporal res: 31 to 86 ms Acquisition time: 5-15 min Reconstruction: <3 hours offline 1-SPIRiT	may facilitate more reliable detection and characterization of intracardiac shunts and valve regurgitation
Schnell et al, MRM 2014[37] n=10 volunteers mean age 28.4 years	3T Venc = 150 cm/s looked at 12 and 32 channel receiver coils **Navigator-gated Cartesian 4D flow with prospective triggering:** SR= 2.1×2.5×2.5 mm^3 tempRes = 40.0 ms GRAPPA accelerated R= 2 n(net acceleration = 1.6) **k-t accelerated cartesian 4D flow with prospective triggering:** matched imaging parameters k-t acceleration rates: 3,5,8 (net acceleration = 2.8, 4.2, 6.3)	Quantification at aortic root, mid AAo, mid arch, proximal DAo. **Differences from GRAPPA R=2** peak flow was significantly different for R=5 and R=8 R = 5: Peak flow: −5.3 to −3.7% R=8: peak flow: −12.0% to −8.0% Peak velocity was only significantly different for R=8: −7.4% at root, −12.0% at DAo p<0.03 net flow similar for all methods
Giese et al. JCMR 2014[32] n=6 for flow measurements	1.5T: Intracardiac: Venc = 200 cm/s for volunteers, Venc = 120-400 cm/s for patients **Navigator-gated, retrospectively gated, k-t PCA-accelerated 3D PC:** nominal acceleration of 8, 11 and 7, SR=2.5×2.5×2.5 mm^3 (volunteers), 1.26-2.31×1.4-2.31, 1.72-2.31 mm^3 (pediatric patients) temporal resolution = 35.6 ±5.3 ms, **Acquisition time:** 5.6 min for volunteers, 3.6 to 7.1 for others,	Volunteers: interested in AAO, MPA, RPA, LPA, SVC; stroke volume/net flow: 5.6± 14.9% difference from 2D flow peak flow: −5.1±7.5% from 2D CHD: 1.6±4.8 mL difference underestimation in net flow,

Study and Population	MRI Acquisitions	Main Relevant Findings
Dvorne et al, Radiology 2015[21] n=10 (7 liver patients, 3 healthy volunteers) Mean age 51 (30-70) years	1.5T Venc = 60 cm/s Abdominal acquisition **Free-breathing, Navigator-gated Cartesian 4D Flow with prospective gating:** acquired SR: 2.5×3.9×5.0 mm^3 TempRes = 68.4 ms; R=2 GRAPPA Acquisition time= 11 min 21 sec (6 min 12 sec-20 min 37 sec) **Accelerated Prospectively Gated 4D flow Spiral sampling with multiple breatholds** Acquired SR = 2.5×2.5×5.0 TempRes = 66.2 ms R=6 Acquistion time: 18-25 s CS reconstruction	Quantified 18 major abdominal vessels: CS reconstruction took 3 hours per subject offline Flow: −2.8 to −38.8% change in flow ($p<0.001$)in CS compared to cartesian 4D flow Peak Velocity: −30.9 to 86% change compared to cartesian ($p=0.024$);
Zaman et al JMRI 2015[38] n=15 healthy subjects (mean 26.5, 22-48 years, 10M), 8 patients with surgically repaired aortic coarctation (4M, 30.5 years, range 22-37 years).	3T: Aorta acquisition **free-breathing retrospectively-gated, cartesian, SENSE 4D flow:** R = 1.6, SR=2.5×2.5×2.5 mm^3 Temporal Resolution = 50-55 ms Acquisition time: 25.2 min **Free-breathing, prospectively gated 4D flow with k-t BLAST:** R=5, SR=2.5×2.5×2.5 temp res 45-60 ms (5.5 min)	Reference was 2D PC using SENSE: no significant differences in flow, velocity, or stroke volume values for any of the 4D flow pulse sequences compared to the reference
Cheng et al, Nature 2017[36] n=6 (3F) age 3 days to 15 years, pediatric patients	1.5/3T, Venc=100-250 cm/s Whole heart acquisition **4D flow with intrinisic butterfly navigators, Vrad sampling, and CS:** SR=0.9-2.1×0.8-2.0×1.4-3.0 mm^3 TR/TE=1.7-1.8 ms/ 4.0-5.8 ms Acquisition time: 7:14 to 10:34 min	Comparison of patients found lower average flow that varies throughout time in XD flow recon (~0.25 L/min) compared to conventional (~0.35 L/min) but also improved image sharpness and decreased velocity standard deviations in XD flow.
Bollache et al, MRM 2018[33] n=20 (10 volunteers, mean age 61 [31-77] years; 10 patients with aortic disease, mean age 60 [44-74] years; in-vitro: pulsatile 3D printed aortic flow phantom with aortic coarctation	1.5 T Aortic acquisition Venc = 150/150-250 cm/s (volunteers/patients) **Navigator-gated Cartesian 4D flow with prospective triggering:** acquired SR =3.1×2.1×2.6 mm^3 (is it acquried) TempRes = 38.4-39.2 ms Acquisition time (average): 11:56-12:47 **k-t accelerated cartesian 4D flow with prospective triggering and varying samping patterns (R=5):** *Volunteers:* acquiredSR: 3.4×2.3×2.6-3.3 and 4.5×2.3×2.6-3.8 mm^3 tempRes: 67.2 ms Acquisition time: 3:00 min *Patients:* acquired SR: 3.4×2.3×2.8-3.0 mm^3 TempRes = 65.6 ms Acquisition time: <2:30 min	differences from GRAPPA R=2 **In vitro:** Peak Velocity: −22 to −0.8% Peak Flow: −4.0 to 4.2% Net flow: −2.0 to 11% ***Healthy Volunteers:*** Peak Velocity: −18 to 6.4% PeakFlow: −15.0 to 3.0 % Net flow: −17.0 to 2.9% **Patients:** Peak Velocity: −5.0 to −3.8% Peak Flow: −4.1 to − 3.8% Net Flow: 4.4 to 5.8%